Nano Energy 27 (2016) 247–254

Contents lists available at ScienceDirect

Nano Energy

journal homepage: www.elsevier.com/locate/nanoen

Hierarchical NiMo-based 3D electrocatalysts for highly-efficient hydrogen evolution in alkaline conditions

Ming Fang [a,c,1], Wei Gao [a,b,c,1], Guofa Dong [a,c], Zhaoming Xia [b], SenPo Yip [a,c,d], Yuanbin Qin [e], Yongquan Qu [b,e,f,*], Johnny C. Ho [a,c,d,**]

[a] Department of Physics and Materials Science, City University of Hong Kong, 83 Tat Chee Avenue, Kowloon, Hong Kong
[b] Center for Applied Chemical Research, Frontier Institute of Science and Technology, Xi'an Jiaotong University, Xi'an 710049 , PR China
[c] Shenzhen Research Institute, City University of Hong Kong, Shenzhen 518057, PR China
[d] State Key Laboratory of Millimeter Waves, City University of Hong Kong, 83 Tat Chee Avenue, Kowloon, Hong Kong
[e] State Key Laboratory for Mechanical Behavior of Materials, Xi'an Jiaotong University, Xi'an 710054, PR China
[f] MOE Key Laboratory for Nonequilibrium Synthesis and Modulation of Condensed Matter, Xi'an Jiaotong University, Xi'an 710049, PR China

ARTICLE INFO

Article history:
Received 18 April 2016
Received in revised form
7 June 2016
Accepted 5 July 2016
Available online 5 July 2016

Keywords:
Electrocatalysis
Nickel-molybdenum alloys
Hierarchical nanostrutures
Hydrogen evolution

ABSTRACT

In recent years, electro- or photoelectrochemical water splitting represents a promising route for renewable hydrogen generations but still requires the substantial development of efficient and cost-effective catalysts to further reduce the energy losses and material costs for scalable and practical applications. Here, we report the design and development of a hierarchical electrocatalyst constructed from microporous nickel foam and well-assembled bimetallic nickel-molybdenum (NiMo) nanowires, which are capable to deliver current densities as comparable to those of the state-of-the-art Pt/C catalyst at low overpotentials and even larger current densities at higher overpotentials ($>$ 124 mV). This binder-free 3D hydrogen evolution cathode catalyst also exhibits the excellent stability, without any decay of the current density observed after long-term stability tests at a low current density of 10 mA cm^{-2} and a high current density of 50 mA cm^{-2}. By pairing this NiMo 3D cathode with a NiFe-based anode, a water electrolyzer can be achieved with a stable current density of 10 mA cm^{-2} for overall water splitting at a voltage of $\sim$1.53 V, indicating that the water splitting can be indeed realized without any performance sacrifice by using earth abundant electrocatalysts.

1. Introduction

Hydrogen, as an important chemical feedstock widely used in petroleum refining and ammonia synthesis [1,2], has been proposed as an alternative energy carrier in future in order to alleviate human's reliance on fossil fuels as well as to lower the global carbon emissions [3,4]. However, the current production of hydrogen is still mostly achieved with the steam reforming process of fossil fuels at high temperatures [5,6]. In this regard, significant amount of attention has been attracted to produce hydrogen through electrolysis of water (i.e. $2H_2O \rightarrow H_2 + O_2$) and ideally to drive it by a renewable energy source, such as solar and wind power. The hydrogen evolution reaction (HER, i.e. $2\,H^+ + 2e^- \rightarrow H_2$ in acidic conditions and $2\,H_2O + 2e^- \rightarrow H_2 + 2OH^-$ in alkaline conditions) is a fundamental step in this water splitting. Generally, efficient hydrogen evolution requires the use of a catalyst to minimize kinetic barriers imposed by the high activation energies for the formation of reaction intermediates on the electrode surface, which can reduce the overpotential required to drive the reaction at a significant rate [7,8]. Up to now, the best known HER catalyst is platinum, but the scarcity and high cost have prohibited its large-scale commercial utilizations; therefore, researchers have now devoted to introducing efficient non-noble-metal catalysts for HER. According to the Sabatier principle [9] of electrocatalysis, the electrocatalytic activity of catalysts is depended on the heat of adsorption of the reaction intermediate on the electrode surface. For HER, the activity follows a volcano-type relation in which the best catalysts have hydrogen binding free energies (ΔG_H) closest to the optimum value of zero, as that exhibited by Pt [10]. It is suggested that a combination of two non-noble metals from the two brunches of volcano curve could result in the enhanced activity [11–15]. Some latest literatures also reported the high performances of binary and ternary metal composites in hydrogen generation, like CoSn, CoSnZn, and NiMo, etc. [16–19]. In specific,

* Corresponding author at: Center for Applied Chemical Research, Frontier Institute of Science and Technology, Xi'an Jiaotong University, Xi'an 710049, PR China
** Corresponding author at: Department of Physics and Materials Science, City University of Hong Kong, 83 Tat Chee Avenue, Kowloon, Hong Kong
E-mail addresses: yongquan@mail.xjtu.edu.cn (Y. Qu), johnnyho@cityu.edu.hk (J.C. Ho).
[1] These authors contributed equally to this work.

http://dx.doi.org/10.1016/j.nanoen.2016.07.005
2211-2855/

nickel has been proposed as a good candidate catalyst for HER due to its smaller ΔG_H as compared to other earth-abundant metals. Moreover, by alloying nickel with transition metals on the left hand side of the periodic table (i.e. W, Mo, Fe), an increase in the intrinsic electrocatalytic activity in the HER, as compared to pure nickel, can be obtained [12,20–22]. Among all binary metal compounds, NiMo alloys have been reported as the most active electrocatalysts for HER in alkaline conditions [18,19,22–24]. Nonetheless, previous methods in synthesizing Ni-containing catalytic alloys usually involves cathodic deposition processes, which comes with the low controllability over their morphologies and chemical compositions [21,25]. Due to the existing problems in these synthesis methods, the corresponding performances of reported Ni-Mo catalysts are still much lower than that of state-of-that-art precious Pt/C catalysts. Recently, McKone et al. [26] have demonstrated that ultrafine amorphous NiMo nanopowders synthesized by chemical reduction from Ni-Mo oxide precursors have much improved activity for HER in alkaline conditions, indicating that there is much room for further improving the performance of NiMo catalysts by manipulating their aggregation states. Previous studies have also illustrated that the rational assembly of low-dimensional building blocks such as 1D nanorods or nanowires (NWs) into 3D hierarchical architectures is an effective strategy for designing highly-efficient HER catalysts [27–33]. As compared to randomly segregated particles on planar substrates, the well-ordered low-dimensional nanowires or nanorod arrays grown on 3D substrates may offer many advantages for catalysis, including the increased catalyst loading amount and surface area, reduced internal resistance, shortened ionic diffusion path, and favorable boundary for gas bubble release.

In this report, we demonstrate the fabrication of hierarchically architected HER catalysts consisting of well-assembled porous nickel-molybdenum nanowire (NiMo-NW) arrays grown on 3D Ni foam. Such hierarchical catalyst (denoted as NiMo-NWs/Ni-foam) can be easily achieved via well-established chemical processes, including a hydrothermal process to synthesis the $NiMoO_4$ precursor and a subsequent thermal reduction step to obtain the final metal alloys. As expected, the NiMo-NWs/Ni-foam catalyst exhibits a respectably high catalytic activity for HER in alkaline conditions, delivering comparable current densities to those of the state-of-the-art Pt/C catalyst at low overpotentials and even larger current densities at higher overpotentials (i.e. >124 mV). The obtained catalyst as well shows the excellent stability without any obvious decay of the current density observed after long-term stability tests at a low current density of 10 mA cm^{-2} and a high current density of 50 mA cm^{-2}. More importantly, when paring the NiMo-NWs/Ni-foam cathode with a nickel foam anode that loaded with nickel-iron layered double hydroxide (NiFe LDH) nanosheets, an impressively small voltage of $\sim$1.53 V is only required in order to realize the overall electrochemical water splitting in 1 M KOH with a stable current density of 10 mA cm^{-2}, illustrating the promising potency of NiMo-NWs/Ni-foam as the highly-efficient HER electrode.

2. Experimental section

2.1. Preparation of NiMo-NWs/Ni-foam

In this work, the Ni foam (1×3 cm) was cleaned successively in diluted HCl (10%), DI water, acetone and ethanol for 15 min with ultrasonication, and then dried by nitrogen gas. $NiMoO_4$ nanowires (NWs) were grown on the Ni foam through a previously reported hydrothermal process [34]. Briefly, the cleaned nickel foam was placed inside a Teflon-lined stainless steel autoclave which contained 1 mmol $NiCl_2 \cdot 6H_2O$, 1 mmol $Na_2MoO_4 \cdot 2H_2O$ and 15 mL deionized water, and the growth of $NiMoO_4$ nanomaterials was performed by heating the autoclave at 160 °C for 6 h within an electric oven. After cooling down to room temperature, the Ni foam coated with $NiMoO_4$ NWs was taken out of the autoclave, followed by the thorough washing with deionized water and ethanol alternatively with the assistance of ultrasonication to remove any absorbed residuals, and then dried at 60 °C. In order to obtain NiMo alloy NWs, the as-prepared $NiMoO_4$ NWs supported on the Ni foam was placed in a tube furnace and heated at 500 °C for 1 h with the temperature ramping of 3 °C min^{-1} under an Ar/H_2 (200/50 sccm) environment. After cooling down to room temperature, the H_2 was stopped and the sample was passivated by dilute oxygen gas (a mixture gas of 2 sccm O_2 and 198 sccm Ar) for 30 min to avoid the radical oxidization or auto-igniting upon the exposure in air.

2.2. Characterization

The morphologies of as-prepared $NiMoO_4$ nanomaterials supported on the Ni foam and NiMo-NWs/Ni-foam were investigated by scanning electron microscopy (SEM, Philips XL30 FEG) with an accelerating voltage of 10 kV, transmission electron microscopy (TEM) and high-resolution TEM (HRTEM, JEOL JEM 2100F) with an accelerating voltage of 200 kV. The phase purity was examined by X-ray diffractometer (XRD, Philips) using Cu Kα radiation ($\lambda = 0.15406$ nm). To gain better resolution, the sample was pressed into a compact sheet before the XRD measurement. The element analysis was also determined by energy dispersive X-ray spectroscopy (EDS, Oxford Instrument and EDAX Inc.).

2.3. Electrochemical measurements

Electrochemical measurements were carried out on a Gamry G300 potential station. Before tests, an active area for contacting with the electrolyte was defined by applying the silicon rubber. The electrochemical activity and stability tests were then performed in 1 M KOH (pH=13.71) with a three-electrode configuration where NiMo-NWs/Ni-foam, Ni plate and saturated calomel electrode (SCE) were used as the working electrode, counter electrode and reference electrode, respectively. Linear sweeping voltammetry (LSV) and cyclic voltammetry (CV) curves were measured at a scan rate of 5 mV s^{-1}. Unless otherwise noted, all the tests were performed with iR corrections using the current interrupt method as provided by the potential station. The loading mass of the NiMo alloy was 0.41 mg cm^{-2}, determined by careful weighting. Both sides of the nickel foam were taken into account for the area calculation. As a control, the commercial Pt/C (20% Pt on Vulcan XC-72 R) catalyst loaded on a polished glass carbon electrode was also measured under the identical condition. In specific, the Pt/C electrode was prepared by first dispersing Pt/C powder in a Nafion solution and then dropping it on the polished glassy carbon electrode and dried in the open air. The loading density of Pt/C powder is $\sim$0.61 mg cm^{-2} [35]. Also, the potential scale was corrected with respect to the reversible hydrogen electrode (RHE) according to the Nernst equation ($E_{vs\ RHE} = E_{vs\ SCE} + 0.059 \times pH + 0.242$). The calculated value is 1.051, which is consistent with the potential difference measured between the SCE and a freshly polished Pt foil under H_2 gas purge in 1 M KOH. For water electrolysis, a two-electrode configuration was set up where the NiMo-NWs/Ni-foam was used as the cathode while the NiFe LDH /Ni foam was used as the anode.

3. Results and discussion

In general, the precipitation reaction between Ni^{2+} and MoO_4^{2-} yields the stoichiometric $NiMoO_4$ oxide compound. By

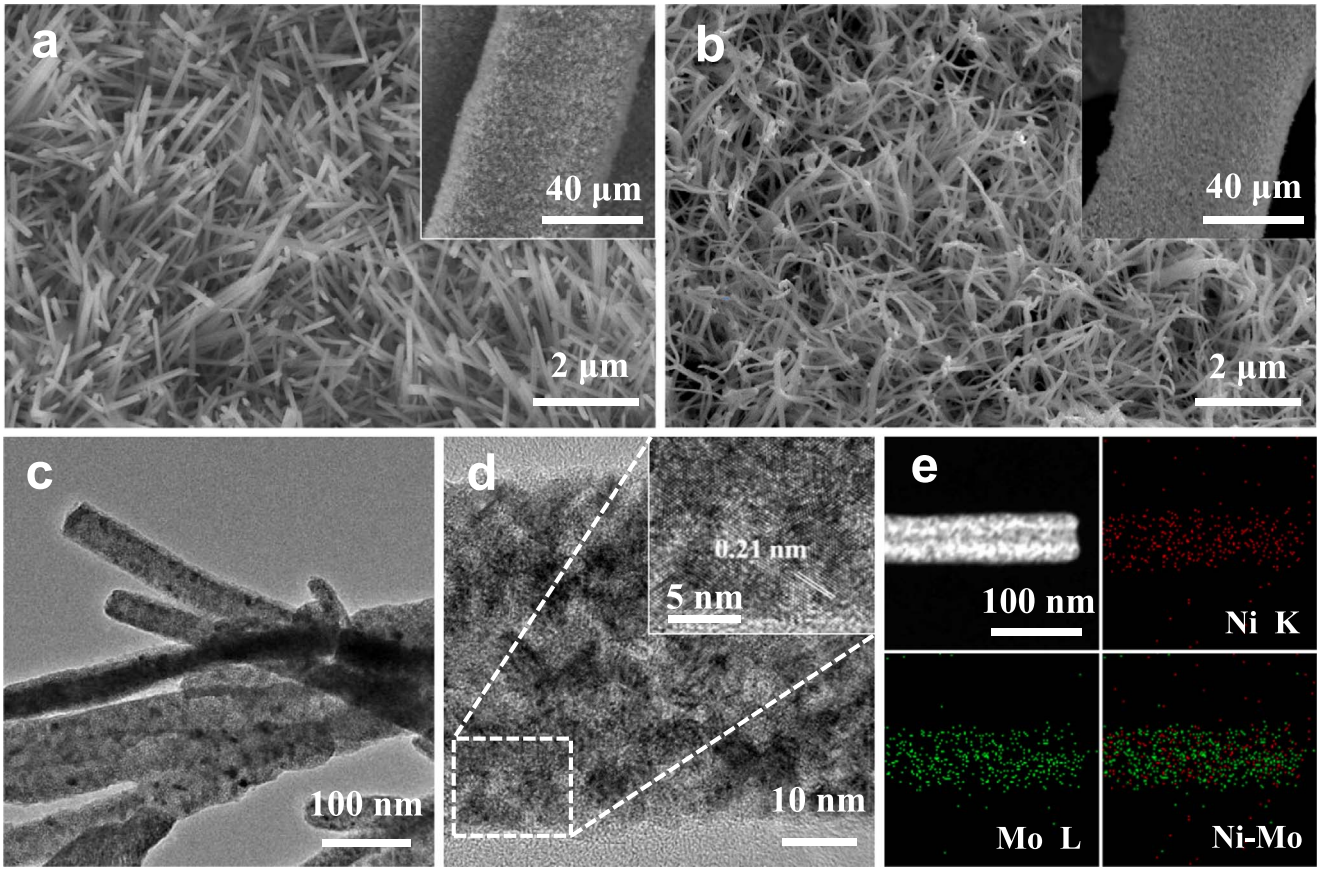

Fig. 1. (a) SEM images of $NiMoO_4$ NWs on Ni foam. (b) SEM images of NiMo NWs on Ni foam. The insets in (a, b) show large-area views. (c) TEM image of NiMo NWs. (d) HRTEM image of a NiMo NW. The inset shows a zoom-in view. (e) STEM and corresponding elemental mapping images of part of a single NiMo NW.

controlling the reaction condition, high aspect-ratio $NiMoO_4$ NW arrays can be grown on different conductive substrates through a simple hydrothermal process [34]. In this study, we utilize the $NiMoO_4$ NWs as precursors for the synthesis of bimetallic Ni-Mo alloys with identical elemental distributions. Fig. 1a gives the SEM images of $NiMoO_4$ NWs supported on the microporous Ni foam grown via the hydrothermal method. It reveals that the as-synthesized NWs are near-vertically aligned and uniformly packed on the nickel substrate with lengths of several micrometers and diameters of tens of nanometers. XRD characterization on the sample discloses two groups of peaks (Fig. S1, Electronic Supplementary Information, ESI), with one group corresponding to the Ni foam substrate (44.2°, 51.5° and 76.1°) while another group indexed to the monoclinic $NiMoO_4$ materials (13.4°, 26.6° and 29.3°, JCPDS No. 86–0361), suggesting that the obtained NWs are composed of $NiMoO_4$ in the stoichiometry.

The $NiMoO_4$ NWs are then reduced into metallic alloys as the catalyst. Fig. 1b depicts the SEM images of the samples thermally reduced in the H_2/Ar atmosphere. Although the NWs become curved, the wire-like morphology was well preserved without collapsing. Further investigation in TEM reveals that there are many tiny voids or pores residing inside the NWs which are possibly evolved by the loss of hydration or oxygen during the thermal reduction process (Fig. 1c and d). Such pores would be beneficial to the catalytic reaction by providing more exposed active sites. Fig. 1d inset also shows that the NiMo NWs had clear lattice fringes with an interplanar distance of 0.209 nm, corresponding to the (331) plane of the NiMo alloy, while Fig. 1e displays the scanning TEM (STEM) image of NiMo alloy NWs and their corresponding EDS elemental mapping images (the EDS spectrum is shown in Fig. S2, ESI), confirming the uniform distribution of Ni and Mo elements in the NWs. Therefore, all these above results can evidently confirm the formation of NiMo alloy NWs with uniform distributions of the metal elements here.

The electrochemical hydrogen evolution activity of the obtained NiMo-NWs/Ni-foam is then measured in 1 M KOH electrolyte using a three-electrode system. A Ni plate is used as the counter electrode to avoid any possible metallic contamination on the investigated catalysts. Fig. 2a presents the iR-corrected polarization curves of the bare Ni foam, the NiMo-NWs/Ni-foam catalyst, and the Pt/C control sample. As anticipated, the bare Ni foam displays a relatively low catalytic activity which requires an overpotential of $\sim$270 mV to drive a current density of 10 mA cm^{-2}. In contrast, the NiMo-NWs/Ni-foam catalyst exhibits the excellent catalytic activity, demonstrating a negligible onset potential for hydrogen evolution in the electrolyte. An overpotential of only $\sim$30 mV is required for the electrode to drive a current density of 10 mA cm^{-2}, which is much smaller than the one recently reported by utilizing the amorphous NiMo nanopowders [26] and other non-noble electrocatalysts for HER in alkaline solutions, as summarized in Table S1 (ESI). This value is already close to the overpotential of 34 mV to achieve the same current density (10 mA cm^{-2}) for the state-of-the-art Pt/C catalyst tested in the same electrolyte. Notably, it has also been observed that the polarization curve of the NiMo-NWs/Ni-foam catalyst intersects with that of the Pt/C electrode at 125 mV with the corresponding current density of $\sim$100 mA cm^{-2} and illustrates the higher current densities at overpotentials afterwards, indicating that the NiMo-NWs/Ni-foam catalyst has the superior catalytic performance at higher overpotentials.

To shed light on insights about the reaction kinetics, the detailed Tafel analysis is performed. The Tafel equation is given by

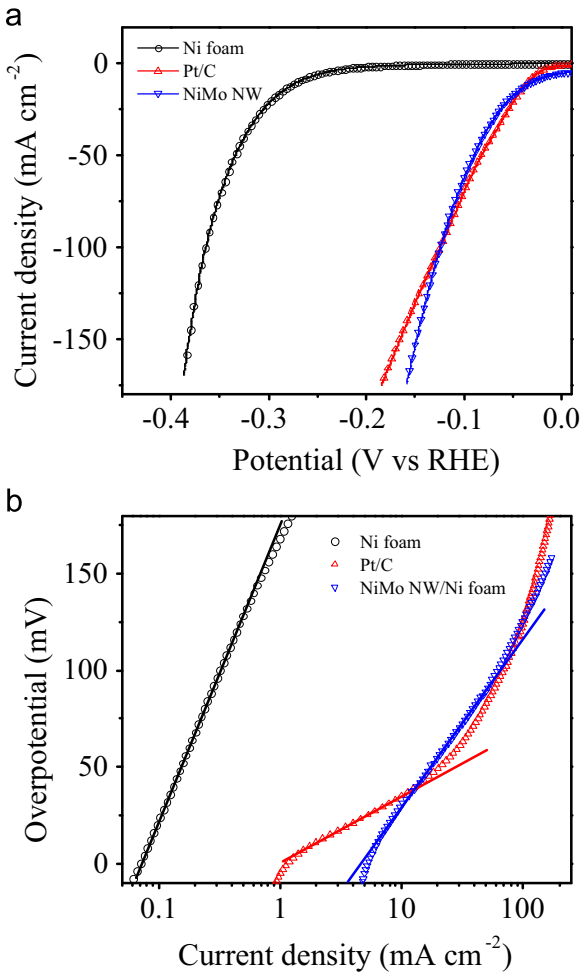

Fig. 2. (a) Polarization curves and (b) corresponding Tafel plots of Ni foam, NiMo NWs/Ni foam and commercial Pt/C in 1 M KOH solution with scan rate of 5 mV s^{-1}.

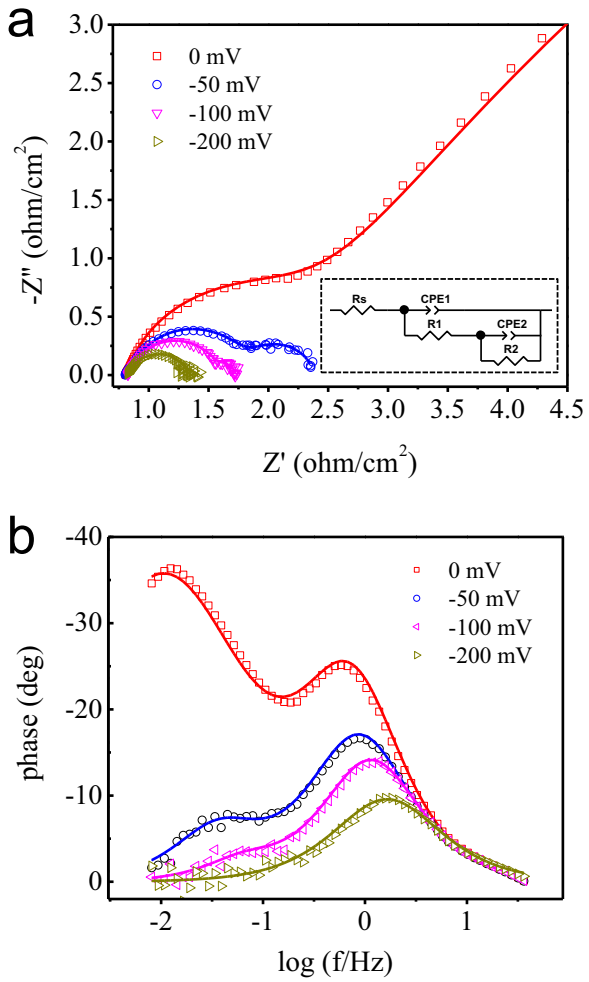

Fig. 3. (a) Nyquist and (b) bode plots of EIS at different overpotentials. The scattered symbols represent the experimental results and the solid lines are simulation fitted results. The inset at the bottom of (a) shows the equivalent circuit for the simulation.

$$\eta = b\ log(j/j_0) \quad (1)$$

where j is the current density, j_0 is the exchange current density (i.e. a constant at $\eta = 0$ V) and b is the Tafel slope. The equation suggests that ideal catalysts should have both low Tafel slopes and high exchange current densities. Fig. 2b presents the Tafel plots of the tested catalysts. By fitting the linear region, Tafel slopes of 154, 86 and 34 mV dec^{-1} are yield for the bare Ni foam, NiMo-NWs/Ni-foam and Pt/C, respectively, indicating that the NiMo-NWs/Ni-foam has much higher intrinsic activity than the one of bare Ni foam for HER while still being less active than the Pt/C catalyst. However, as shown in the graph, while both curves for the bare Ni foam and the NiMo-NWs/Ni-foam are dominated by linear relationships in the presented η range, the curve for the Pt/C only follows the linear relationship at the low η region ($0 < \eta < 50$ mV) and deviated dramatically for the higher η regions ($\eta > 50$ mV). As a result, the Pt/C shows the lower activity than that of the NiMo-NWs/Ni-foam. This change is likely due to the increased effect of gas bubbling which blocks the contact between the catalyst and the electrolyte. Such effect is largely mitigated in the NiMo-NWs/Ni-foam electrode owing to the 3D porous microstructure of the Ni foam and the wire-like morphology of the NiMo catalysts, both of them are favorable for the effective mass transfer, so that the NiMo-NWs/Ni-foam can exhibit the better catalytic activity at higher overpotentials. In alkaline conditions, hydrogen evolution on a metal surface consists of two primary steps. The first one typically involves an electron transfer process that yields an intermediate adsorbed hydrogen atom on the catalyst surface ($M + H_2O + e^- \rightarrow M\text{-}H_{ads} + OH^-$, Volmer reaction) while the subsequent one takes in the H_2 formation via either an electrochemical desorption process ($M\text{-}H_{ads} + H_2O + e^- \rightarrow M + H_2 + OH^-$, Heyrovsky reaction) or a recombination process ($2M\text{-}H_{ads} \rightarrow 2M + H_2$, Tafel reaction). According to the kinetic model [36], the Tafel slope of 86 mV dec^{-1} suggests that the HER on the NiMo-NWs/Ni-foam catalyst proceeds via the Volmer-Heyrovsky mechanism and the reaction rate is determined by the electrodesorption (Heyrovsky) step, which is consistent with the previous report [37].

Table 1
Calculated double layer capacitance (C_{DL}), roughness factor (σ) and normalized current density at overpotentials (η) of 0 mV and 100 mV. The unit for capacitance and current densities are mF cm^{-2} and mA cm^{-2}, respectively.

Catalysts	C_{DL}	σ	j_0/σ (η=0 mV)	j/σ at η=100 mV
Ni foam	0.46	11	0.006357	0.027868
NiMo-NWs/Ni-foam	29.42	735	0.006250	0.083726

Electrochemical impedance spectroscopy (EIS) is then employed to better understand the origin of this obtained high electrocatalytic activity of the NiMo-NWs/Ni-foam. Fig. 3 shows the Nyquist and bode plots of the Ni-Mo/Ni-foam electrode at different overpotentials. It is clearly seen that the spectra exhibit

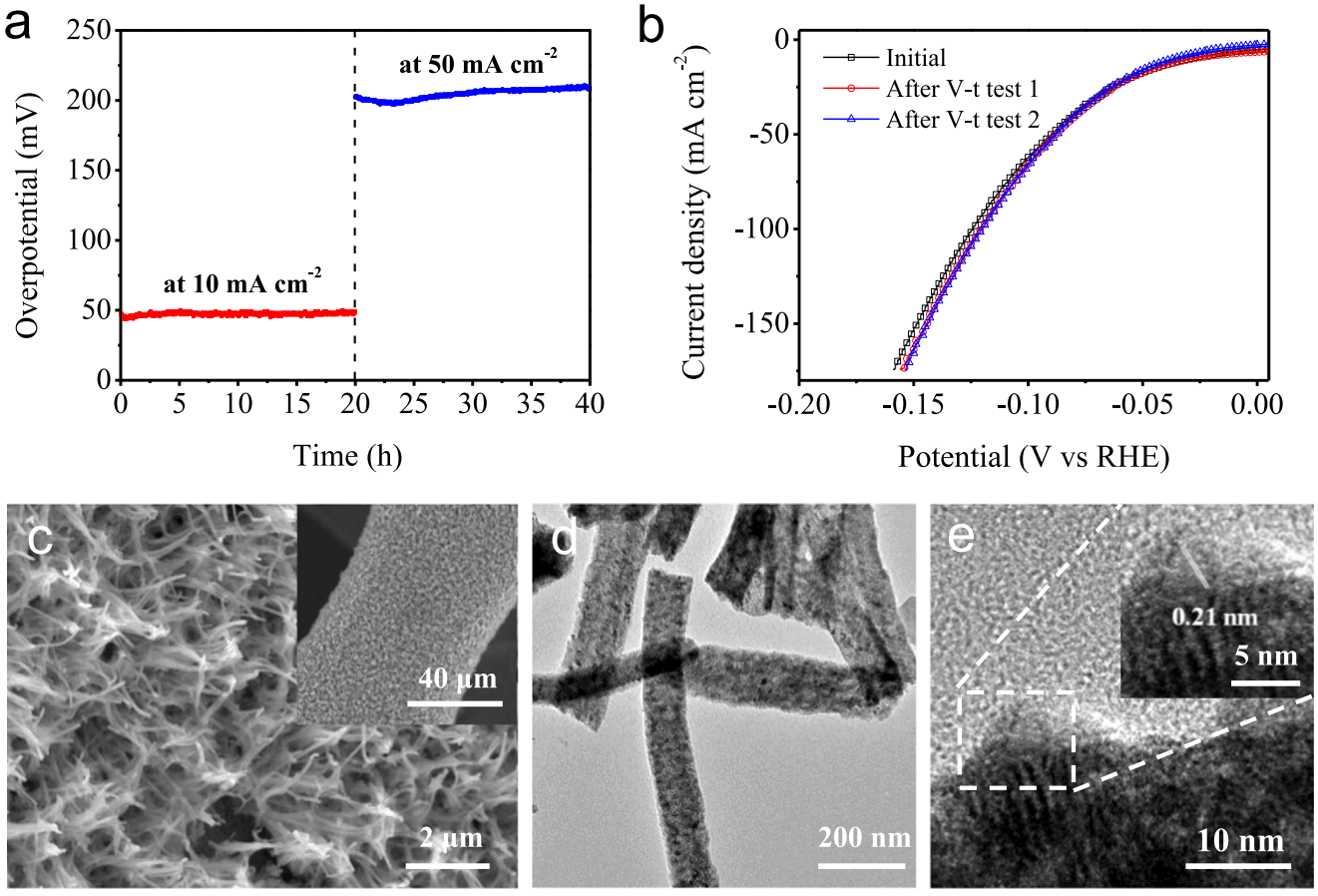

Fig. 4. (a) Chronopotentiometric measurements at current density of 10 mA cm^{-2} for 20 h and another 50 mA cm^{-2} for another 20 h. (b) Polarization curves (with iR corrections) of NiMo NWs/Ni foam after 20 h and 40 h stability test. (c) SEM, (d) TEM and (e) HRTEM images of NiMo NWs/Ni foam sample after 40 h test. Inset in (c) shows a large-area SEM view and inset in (e) is a zoom-in HRTEM image on single NiMo NW after test.

two distinct time constants as indicated by the presence of two distinct semicircles in the Nyquist plots. Both of the circles decreases with the increase of applied overpotentials, which can be described by a two-time constant parallel model (2TP, as shown in the bottom inset of Fig. 3a) that reflects the response of a HER system characterized by two time constants, and both of them are overpotential-dependent [38–40]. Parameters derived from the model are summarized Table S2, ESI. The value of CPE_1 (constant phase element) is shown to be relatively stable with small deviations at different overpotentials, while the value of R_1 decreases dramatically with the increase in overpotential, which coincides well with the characteristic of the charge-transfer kinetics, corresponding to the response of double layer capacitance by CPE_1, and HER charge transfer resistance by R_1. Contrary to the behavior of CPE_1, the value of CPE_2 increases evidently with the increase of overpotential, and meanwhile, the value of R_2 decreases. This is a typical behavior of the response of hydrogen adsorption on an electrode surface. As a result, our EIS analysis confirms the existence of the M-H_{ads} layer formation. In other words, the first reaction step (Volmer reaction) that represents the adsorption of hydrogen intermediates can be considered in equilibrium, which is consistent with our previous analysis that the Heyrovsky step is the rate-determining step. EIS results can also be used to estimate the actual surface area of electrocatalytic layers using a value of the double layer capacitance (C_{DL}) [41–43]. The actual value of C_{DL} can be calculated by [44].

$$C_{DL} = \left[Q_0 \left(1/R_s + 1/R_1 \right)^{(a-1)} \right]^{(1/a)} \quad (2)$$

Furthermore, by taking the average C_{DL} of 40 μF cm^{-2} for a smooth metal surface, the roughness factor (σ), that characterizes the real-to-geometrical surface area ratio, can be calculated as $\sigma = C_{DL}/40\ \mu F\ cm^{-2}$. By knowing this important piece of information, it is possible to compare the intrinsic activities of catalysts by normalizing the current density to the electrochemically available surface area. Table 1 compares the calculated values of double layer capacitance, roughness factor and normalized current density (at $\eta = 0$ and 100 mV) of the bare Ni foam and NiMo-NWs/Ni-foam catalyst. The calculated C_{DL} value is 29.41 mF cm^{-2} for the NiMo-NWs/Ni-foam, which equals to ~64 times of that of the bare Ni foam. Interestingly, after normalization, the difference of the exchange current density values of the two samples becomes very small. However, as also displayed in the normalized polarization curves and Tafel plots in Fig. S3, ESI, the NiMo-NWs/Ni-foam catalyst still exhibits the much higher normalized current density at a given overpotential, such as offering 3 times larger normalized current density at the overpotential of 100 mV, indicating that it possesses the higher intrinsic catalytic activity.

The alloying effect of transition metals on HER catalytic activity has been extensively discussed in previous studies. In general, two possible mechanisms have been proposed for this activity enhancement [20,45]. The first mechanism involves electronic synergy, like an electron average effect between the two metal components, in which intermetallic bonding results in a more favorable energy state for both the primary step of hydrogen adsorption and the following step for the formation of hydrogen molecules [20,46–48]. The second mechanism involves the well-known 'spillover' effect as that has been proposed in many heterogeneous catalyzing processes [49]. In this mechanism, one of

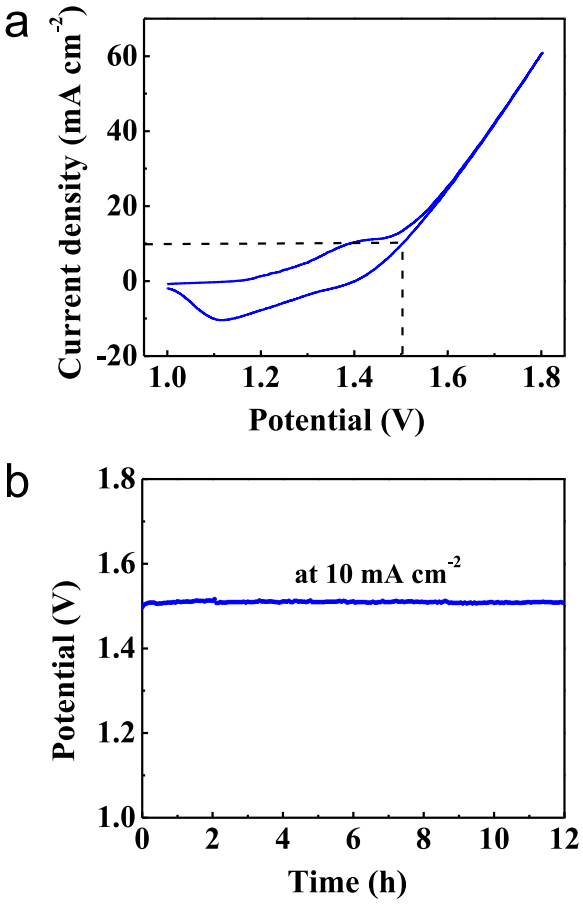

Fig. 5. (a) CV curve (without iR correction) of a two-electrode cell with a NiMo-NWs/Ni-foam cathode and a NiFe-LDH/Ni-foam anode in 1 M KOH with scan rate of 5 mV s^{-1}. (b) Long-term stability test with the current density of 10 mA cm^{-2} in 1 M KOH solution.

the metal components facilitates the adsorption of hydrogen intermediates and delivers the bound hydrogen atoms to the other metal component through hydrogen spill over. The HER is then finished on this second component. In this way, the two components can work cooperatively to catalyse the HER reaction with enhanced activity. These proposed mechanisms would lend to further insight into the mechanism of the improvement in intrinsic catalytic activity of our NiMo catalyst.

Apart from the catalytic activity, stability is another important requirement of catalysts for the HER system. In this case, long-term stability of our NiMo-NWs/Ni-foam electrocatalyst is assessed in 1 M KOH at constant current densities. Fig. 4a gives the time-dependent overpotential curves (without iR correction) of the NiMo NWs/Ni foam tested for 20 h at the current density of 10 mA cm^{-2} and another 20 h at 50 mA cm^{-2}. Slight increase of the overpotential has been observed during the V-*t* tests (Fig. 4a); however, polarization curves recorded after each test indicate that there is not any decay, instead, a slight improvement of the catalytic activity of the electrode after the first V-*t* test (Fig. 4b). This slight increase of the catalytic activity was possibly owing to the reduction of surface oxides during the initial period of hydrogen evolution, while the observed increase in overpotential as shown in Fig. 4a could be an result of increase mass exchange resistance due to the continuously gas bubbling. In addition, SEM and TEM images presented in Fig. 4c-e do not illustrate any noticeable change in morphology and lattice fringes of the catalyst after the V-*t* tests. Also, the EDS elemental mapping images (Fig. S4, ESI) of obtained NWs further proved that the Ni and Mo elements are still uniformly distributed after the test. All these results confirm the good stability of our NiMo-NWs/Ni-foam electrocatalyst for HER in alkaline conditions.

As encouraged by this impressively high catalytic performance of the NiMo-NWs/Ni-foam, we attempt to build a water electrolyzer for water splitting without employing any noble metal catalysts. Recent studies have shown that nickel-iron based layered double hydroxides (NiFe-LDH) are highly active electrocatalysts for OER [50], and therefore it was utilized as the anode material in our prototype electrolyzer. NiFe-LDH was synthesized by a hydrothermal method using Ni foam as the support substrate [51]. Typical SEM images show that the NiFe-LDH sheets are vertically aligned on the substrate (Fig. S5a, ESI), and polarization curves and Tafel plot of the NiFe-LDH/Ni foam indicate that they have excellent catalytic OER activities (Fig. S5b,c, ESI). The CV curve of the two-electrode electrolyzer (NiFe LDH/Ni foam‖NiMo NWs/Ni foam) without iR correction was then tested in 1 M KOH solution, as exhibited in Fig. 5a. Due to the good activities of both anode and cathode, a geometrical current density of 10 mA cm^{-2} can be realized at a cell potential of 1.53 V in order to produce hydrogen and oxygen simultaneously. A twelve-hour stability test with fixed current density of 10 mA cm^{-2} in 1 M KOH solution is as well witnessed with negligible fluctuation in the cell potential, demonstrating the stable electrocatalytic activity and reliability of our catalysts. Therefore, all these above results have evidently indicated that our hierarchical NiMo-NWs/Ni-foam catalyst can be advantageously utilized in alkaline water electrolysis to drive the water splitting reaction at a significant rate at ultralow overpotentials.

4. Conclusion

In summary, we have successfully prepared the Ni foam supported NiMo alloy nanowires using a simple hydrothermal method followed by a thermal reduction scheme. The unique hierarchical structure and high intrinsic catalytic activity of the alloy make it among the most active catalysts for HER in alkaline conditions. This alloy catalyst can achieve a geometrical current density of 10 mA cm^{-2} with a very low overpotential of 30 mV in alkaline solutions, with the Tafel slope of 86 mV dec^{-1}. Long-term hydrogen evolution tests at current densities of 10 and 50 mA cm^{-2} further prove the excellent stability in alkaline solutions, where the nanowire-like morphology and NiMo alloy structure of this electrocatalyst are still well reserved. With the combination of cathode of NiMo-NWs/Ni-foam and the anode of NiFe-LDH/Ni-foam, a current density of 10 mA cm^{-2} can be realized in the overall water splitting cell and more importantly, this performance can be preserved for at least 12 h with a voltage of ~1.53 V. As a result, all these observed superior catalytic activity and stability of the NiMo MWs/Ni-foam electrocatalyst have made it a promising candidate in overall water splitting for practical hydrogen production.

Acknowledgment

This research was supported by the General Research Fund of the Research Grants Council of Hong Kong SAR, China (CityU 11213115), the National 1000-Plan program and the Fundamental Research Funds for the Central Universities (Grant xjj2013102), the Science Technology and Innovation Committee of Shenzhen Municipality (Grant JCYJ-20140419115507588), the City University of Hong Kong (Project No. 9667124) and a grant from the Shenzhen Research Institute, City University of Hong Kong.

Appendix A. Supporting information

Supplementary data associated with this article can be found in the online version at http://dx.doi.org/10.1016/j.nanoen.2016.07.005.

References

[1] G. Lauermann P. Häussinger R. Lohmüller A.M. Watson Hydrogen, 1. Properties and Occurrence, in: Ullmann's Encyclopedia of Industrial Chemistry, Wiley-VCH Verlag GmbH & Co. KGaA Weinheim, Germany, 2013, pp. 1–15.
[2] US Energy Information Administration, The Impact of Increased Use of Hydrogen on Petroleum Consumption and Carbon Dioxide Emissions, 2008.
[3] L. Barreto, A. Makihira, K. Riahi, The hydrogen economy in the 21st century: a sustainable development scenario, Int. J. Hydrog. Energy 28 (2003) 267–284.
[4] N. Demirdoven, Hybrid cars now, fuel cell cars later, Science 305 (2004) 974–976.
[5] J.R. Rostrup-Nielsen, J. Sehested, J.K. Nørskov, Hydrogen and synthesis gas by steam- and CO_2 reforming, Adv. Catal. 47 (2002) 65–139.
[6] M. Ni, D.Y.C. Leung, M.K.H. Leung, A review on reforming bio-ethanol for hydrogen production, Int. J. Hydrog. Energy 32 (2007) 3238–3247.
[7] T.R. Cook, D.K. Dogutan, S.Y. Reece, Y. Surendranath, T.S. Teets, D.G. Nocera, Solar energy supply and storage for the legacy and nonlegacy worlds, Chem. Rev. 110 (2010) 6474–6502.
[8] M.G. Walter, E.L. Warren, J.R. McKone, S.W. Boettcher, Q. Mi, E. a Santori, et al., Solar water splitting cells, Chem. Rev. 110 (2010) 6446–6473.
[9] A.B. Laursen, A.S. Varela, F. Dionigi, H. Fanchiu, C. Miller, O.L. Trinhammer, et al., Electrochemical hydrogen evolution: Sabatier's principle and the volcano plot, J. Chem. Educ. 89 (2012) 1595–1599.
[10] R. Parsons, The rate of electrolytic hydrogen evolution and the heat of adsorption of hydrogen, Trans. Faraday Soc. 54 (1958) 1053.
[11] M.H. Miles, Evaluation of electrocatalysts for water electrolysis in alkaline solutions, J. Electroanal. Chem. Interfacial Electrochem. 60 (1975) 89–96.
[12] M.M. Jaks, Hypo - hyper- d -electronic interactive nature of synergism in catalysis and electrocatalysis for hydrogen reactions, Electrochim. Acta 45 (2000) 4085–4099.
[13] J.K. Nørskov, T. Bligaard, A. Logadottir, J.R. Kitchin, J.G. Chen, S. Pandelov, et al., Trends in the exchange current for hydrogen evolution, J. Electrochem. Soc. 152 (2005) J23.
[14] C.G. Morales-Guio, L.-A. Stern, X. Hu, Nanostructured hydrotreating catalysts for electrochemical hydrogen evolution, Chem. Soc. Rev. 43 (2014) 6555–6569.
[15] J. Greeley, T.F. Jaramillo, J. Bonde, I. Chorkendorff, J.K. Nørskov, Computational high-throughput screening of electrocatalytic materials for hydrogen evolution, Nat. Mater. 5 (2006) 909–913.
[16] R. Solmaz, G. Kardaş, Fabrication and characterization of NiCoZn–M (M: Ag, Pd and Pt) electrocatalysts as cathode materials for electrochemical hydrogen production, Int. J. Hydrog. Energy 36 (2011) 12079–12087.
[17] A. Döner, F. Tezcan, G. Kardaş, Electrocatalytic behavior of the Pd-modified electrocatalyst for hydrogen evolution, Int. J. Hydrog. Energy 38 (2013) 3881–3888.
[18] Y. Wang, G. Zhang, W. Xu, P. Wan, Z. Lu, Y. Li, et al., A 3D Nanoporous Ni-Mo Electrocatalyst with Negligible Overpotential for Alkaline Hydrogen Evolution, Chem. Electro. Chem. 1 (2014) 1138–1144.
[19] M. Wang, Z. Wang, X. Yu, Z. Guo, Facile one-step electrodeposition preparation of porous NiMo film as electrocatalyst for hydrogen evolution reaction, Int. J. Hydrog. Energy 40 (2015) 2173–2181.
[20] E. Navarro-Flores, Z. Chong, S. Omanovic, Characterization of Ni, NiMo, NiW and NiFe electroactive coatings as electrocatalysts for hydrogen evolution in an acidic medium, J. Mol. Catal. A Chem. 226 (2005) 179–197.
[21] C. González-Buch, I. Herraiz-Cardona, E.M. Ortega, J. García-Antón, V. Pérez-Herranz, Development of Ni-Mo, Ni-W and Ni-Co macroporous materials for hydrogen evolution reaction, Chem. Eng. Trans. 32 (2013) 865–870.
[22] I.A. Raj, K.I. Vasu, Transition metal-based hydrogen electrodes in alkaline solution – electrocatalysis on nickel based binary alloy coatings, J. Appl. Electrochem. 20 (1990) 32–38.
[23] C.C.L. McCrory, S. Jung, I.M. Ferrer, S.M. Chatman, J.C. Peters, T.F. Jaramillo, Benchmarking hydrogen evolving reaction and oxygen evolving reaction electrocatalysts for solar water splitting devices, J. Am. Chem. Soc. 137 (2015) 4347–4357.
[24] M.R. Shaner, J.R. McKone, H.B. Gray, N.S. Lewis, Functional integration of Ni-Mo electrocatalysts with Si microwire array photocathodes to simultaneously achieve high fill factors and light-limited photocurrent densities for solar-driven hydrogen evolution, Energy Environ. Sci. 8 (2015) 2977–2984.
[25] N. Krstajic, V. Jovic, L. Gajickrstajic, B. Jovic, A. Antozzi, G. Martelli, Electrodeposition of Ni-Mo alloy coatings and their characterization as cathodes for hydrogen evolution in sodium hydroxide solution, Int. J. Hydrog. Energy 33 (2008) 3676–3687.
[26] J.R. Mckone, B.F. Sadtler, C. a Werlang, N.S. Lewis, H.B. Gray, Ni-Mo nanopowders for efficient electrochemical hydrogen evolution, ACS Catal. 3 (2013) 166–169.
[27] Z. Chen, D. Cummins, B.N. Reinecke, E. Clark, M.K. Sunkara, T.F. Jaramillo, Core-shell MoO_3-MoS_2 nanowires for hydrogen evolution: a functional design for electrocatalytic materials, Nano Lett. 11 (2011) 4168–4175.
[28] Y. Liang, Q. Liu, A.M. Asiri, X. Sun, Y. Luo, Self-supported FeP nanorod arrays: a cost-effective 3D hydrogen evolution cathode with high catalytic activity, ACS Catal. 4 (2014) 4065–4069.
[29] J. Tian, Q. Liu, N. Cheng, A.M. Asiri, X. Sun, Self-supported Cu_3P nanowire arrays as an integrated high-performance three-dimensional cathode for generating hydrogen from water, Angew. Chem. 126 (2014) 9577–9581.
[30] Z. Lu, W. Zhu, X. Yu, H. Zhang, Y. Li, X. Sun, et al., Ultrahigh hydrogen evolution performance of under-water "superaerophobic" MoS_2 nanostructured electrodes, Adv. Mater. 26 (2014) 2683–2687.
[31] M.S. Faber, R. Dziedzic, M. a Lukowski, N.S. Kaiser, Q. Ding, S. Jin, High-performance electrocatalysis using metallic cobalt pyrite (CoS_2) micro- and nanostructures, J. Am. Chem. Soc. 136 (2014) 10053–10061.
[32] Y. Yan, L. Thia, B.Y. Xia, X. Ge, Z. Liu, A. Fisher, et al., Construction of efficient 3D gas evolution electrocatalyst for hydrogen evolution: porous fep nanowire arrays on graphene sheets, Adv. Sci. 2 (2015) 1500120.
[33] F.-X. Ma, H. Bin, B.Y. Xia Wu, C.-Y. Xu, X.W.D. Lou, Hierarchical β-Mo_2C nanotubes organized by ultrathin nanosheets as a highly efficient electrocatalyst for hydrogen production, Angew. Chem. 127 (2015) 15615–15619.
[34] S. Peng, L. Li, H. Bin, S. Madhavi Wu, X.W.D. Lou, Controlled growth of $NiMoO_4$ nanosheet and nanorod arrays on various conductive substrates as advanced electrodes for asymmetric supercapacitors, Adv. Energy Mater. 5 (2015) 1401172.
[35] G. Dong, M. Fang, H. Wang, S. Yip, H.-Y. Cheung, F. Wang, et al., Insight into the electrochemical activation of carbon-based cathodes for hydrogen evolution reaction, J. Mater. Chem. A 3 (2015) 13080–13086.
[36] J.O. Bockris, E.C. Potter, The mechanism of the cathodic hydrogen evolution reaction, J. Electrochem. Soc. 99 (1952) 169.
[37] J.M. Jakšić, M.V. Vojnović, N.V. Krstajić, Kinetic analysis of hydrogen evolution at Ni-Mo alloy electrodes, Electrochim. Acta 45 (2000) 4151–4158.
[38] E.B. Castro, M.J. de Giz, E.R. Gonzalez, J.R. Vilche, An electrochemical impedance study on the kinetics and mechanism of the hydrogen evolution reaction on nickel molybdenite electrodes, Electrochim. Acta 42 (1997) 951–959.
[39] A. Damian, S. Omanovic, Ni and NiMo hydrogen evolution electrocatalysts electrodeposited in a polyaniline matrix, J. Power Sources 158 (2006) 464–476.
[40] L. Birry, A. Lasia, Studies of the hydrogen evolution reaction on Raney nickel-molybdenum electrodes, J. Appl. Electrochem. 34 (2004) 735–749.
[41] I. Herraiz-Cardona, E. Ortega, J.G. Antón, V. Pérez-Herranz, Assessment of the roughness factor effect and the intrinsic catalytic activity for hydrogen evolution reaction on Ni-based electrodeposits, Int. J. Hydrog. Energy 36 (2011) 9428–9438.
[42] R.D. Armstrong, M. Henderson, Impedance plane display of a reaction with an adsorbed intermediate, J. Electroanal. Chem. Interfacial Electrochem. 39 (1972) 81–90.
[43] C.C.L. McCrory, S. Jung, J.C. Peters, T.F. Jaramillo, Benchmarking heterogeneous electrocatalysts for the oxygen evolution reaction, J. Am. Chem. Soc. 135 (2013) 16977–16987.
[44] G.J. Brug, A.L.G. van den Eeden, M. Sluyters-Rehbach, J.H. Sluyters, The analysis of electrode impedances complicated by the presence of a constant phase element, J. Electroanal. Chem. Interfacial Electrochemistry 176 (1984) 275–295.
[45] J.R. McKone, S.C. Marinescu, B.S. Brunschwig, J.R. Winkler, H.B. Gray, Earth-abundant hydrogen evolution electrocatalysts, Chem. Sci. 5 (2014) 865–878.
[46] H. Ezaki, M. Morinaga, S. Watanabe, Hydrogen overpotential for transition metals and alloys, and its interpretation using an electronic model, Electrochim. Acta 38 (1993) 557–564.
[47] C. Fan, Study of electrodeposited Nickel-Molybdenum, Nickel-Tungsten, Cobalt-Molybdenum, and Cobalt-Tungsten as hydrogen electrodes in alkaline water electrolysis, J. Electrochem. Soc. 141 (1994) 382.
[48] M.M. Jaksic, C.M. Lacnjevac, B.N. Grgur, N.V. Krstajic, Volcano plots along intermetallic hypo-hyper-d-electronic phase diagrams and electrocatalysis for hydrogen electrode reactions, J. New Mater. Electrochem. Syst. 3 (2000) 169–182.
[49] J.G. Highfield, E. Claude, K. Oguro, Electrocatalytic synergism in Ni/Mo cathodes for hydrogen evolution in acid medium: a new model, Electrochim. Acta 44 (1999) 2805–2814.
[50] J. Luo, J.-H. Im, M.T. Mayer, M. Schreier, M.K. Nazeeruddin, N.-G. Park, et al., Water photolysis at 12.3% efficiency via perovskite photovoltaics and Earth-abundant catalysts, Science 345 (2014) 1593–1596.
[51] Z. Lu, W. Xu, W. Zhu, Q. Yang, X. Lei, J. Liu, et al., Three-dimensional NiFe layered double hydroxide film for high-efficiency oxygen evolution reaction, Chem. Commun. 50 (2014) 6479–6482.

Ming Fang received his PhD degree in Physics and Materials Science from City University of Hong Kong (CityU) in 2015. His is now a senior research associate at the Department of Physics and Materials Science at CityU. His research focuses on the development of innovative approaches for nanofabrication and exploring their potential applications in the design of high-performance photonic and electro-catalytic devices.

Wei Gao received his Bachelor's degree from the School of Electrical Engineering, Xi'an Jiaotong University, China in 2013. He is now a pH. D. candidate in both Professor Qu's group at Xi'an Jiaotong University and Professor Ho's group at City University of Hong Kong. His research interest is focused on the heterogeneous catalysis and electrochemical catalysis of transition metals.

Guofa Dong received his master degree in physical chemistry from Fuzhou University in 2008 and then worked as a research staff in Fujian Institute of Research on the Structure of Matter, Chinese Academy of Sciences from 2008 to 2012. During this period his research was most on preparation, functionalization and application of carbon nanomaterials. He then received his PhD in Physics and Materials Science from City University of Hong Kong in 2016. Now his research interests mainly include water splitting through electrochemical or photocatalytic routes, and oxygen reduction reaction in fuel cells.

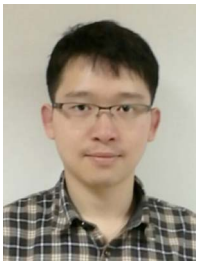

Zhaoming Xia received his Bachelor's degree from the School of Energy and Power Engineering, Xi'an Jiaotong University, China in 2013. Now he is a pH. D. candidate in Professor Yongquan Qu's group. His research interest focuses on first-principle calculations of materials design in catalysis.

SenPo Yip received his BEng in Materials Engineering from City University of Hong Kong and is currently a pH. D student at Department of Physics and Materials Science, City University of Hong Kong under the supervision of Dr. Johnny Ho. His research interests include the synthesis of III-V nanowires and their application for electrical and photovoltaics devices.

Yuanbin Qin received his Ph. D. degree from Institute of Physics, Chinese Academy of Sciences, China in 2011. He is now an engineer in charge of transmission electron microscopy (TEM) in School of Materials Science and Engineering, Xi'an Jiaotong University.

Yongquan Qu received his Ph. D. from the University of California, Davis. He became a faulty member of Center for Applied Chemical Research, Frontier Institute of Science and Technology, Xi'an Jiaotong University, China at 2012. His research is focused on the heterogeneous catalysis in areas of organic synthesis, clean energy production and environmental remediation. Details can be found at http: http://gr.xjtu.edu.cn/web/yongquan/home.

Johnny C. Ho received his B. S.degree with high honors in Chemical Engineering, and M. S. and Ph. D. degrees in Materials Science and Engineering from the University of California, Berkeley, in 2002, 2005 and 2009, respectively. From 2009 to 2010, he worked in the nanoscale synthesis and characterization group at Lawrence Livermore National Laboratory, California. Currently, he is an Associate Professor of Physics and Materials Science at the City University of Hong Kong. His research interests focus on the synthesis, characterization, integration and device applications of nanoscale materials for various technological applications, including nanoelectronics, sensors and energy harvesting. Details can be found at: http://www.ap.cityu.edu.hk/personal-website/johnny/site_flash/index.html.